Cancer Research

Germline Mutations in the Mitochondrial 2-Oxoglutarate/Malate Carrier *SLC25A11* Gene Confer a Predisposition to Metastatic Paragangliomas

Alexandre Buffet[1,2], Aurélie Morin[1,2], Luis-Jaime Castro-Vega[1,2], Florence Habarou[2,3], Charlotte Lussey-Lepoutre[1,2], Eric Letouzé[2,4,5,6,7], Hervé Lefebvre[8], Isabelle Guilhem[9], Magalie Haissaguerre[10], Isabelle Raingeard[11], Mathilde Padilla-Girola[1], Thi Tran[1,2], Lucien Tchara[3], Jérôme Bertherat[2,12,13], Laurence Amar[1,2,13,14], Chris Ottolenghi[2,3], Nelly Burnichon[1,2,15], Anne-Paule Gimenez-Roqueplo[1,2,13,15], and Judith Favier[1,2]

Abstract

Comprehensive genetic analyses have identified germline *SDHB* and *FH* gene mutations as predominant causes of metastatic paraganglioma and pheochromocytoma. However, some suspicious cases remain unexplained. In this study, we performed whole-exome sequencing of a paraganglioma exhibiting an *SDHx*-like molecular profile in the absence of *SDHx* or *FH* mutations and identified a germline mutation in the *SLC25A11* gene, which encodes the mitochondrial 2-oxoglutarate/malate carrier. Germline *SLC25A11* mutations were identified in six other patients, five of whom had metastatic disease. These mutations were associated with loss of heterozygosity, suggesting that *SLC25A11* acts as a tumor-suppressor gene. Pseudohypoxic and hypermethylator phenotypes comparable with those described in *SDHx*- and *FH*-related tumors were observed both in tumors with mutated *SLC25A11* and in *Slc25a11*$^{\Delta/\Delta}$ immortalized mouse chromaffin knockout cells generated by CRISPR-Cas9 technology. These data show that *SLC25A11* is a novel paraganglioma susceptibility gene for which loss of function correlates with metastatic presentation.

Significance: A gene encoding a mitochondrial carrier is implicated in a hereditary cancer predisposition syndrome, expanding the role of mitochondrial dysfunction in paraganglioma. *Cancer Res; 78(8); 1914–22. ©2018 AACR.*

Introduction

Pheochromocytomas and paragangliomas (PPGL) are neuroendocrine tumors with a very strong genetic component. Up to 40% of patients with PPGL carry a germline mutation in one of the 13 susceptibility genes reported so far (two proto-oncogenes and 11 tumor-suppressor genes; for review, see ref. 1). Mutations in *SDHx* genes (*SDHA, SDHB, SDHC, SDHD*), encoding the tricarboxylic acid (TCA) cycle enzyme succinate dehydrogenase (or mitochondrial complex II) account for approximately 50% of the germline mutations identified in affected patients and cause multiple or metastatic PPGL (2). These mutations abolish succinate dehydrogenase (SDH) activity, resulting in the accumulation of its substrate, succinate, which acts as an oncometabolite by inhibiting 2-oxoglutarate (2-OG)–dependent dioxygenases. These include hypoxia-inducible factors (HIF) prolyl-hydroxylases (PHD), ten-eleven translocation enzymes (TET) DNA demethylases (which catalyze the conversion of 5-methylcytosine (5-mC) into 5-hydroxymethylcytosine (5-hmC; ref. 3) and JmjC-domain containing histone demethylases (which promote

[1]INSERM, UMR970, Paris-Centre de Recherche Cardiovasculaire, Paris, France; Equipe labellisée Ligue contre le Cancer. [2]Université Paris Descartes, PRES Sorbonne Paris Cité, Faculté de Médecine, Paris, France. [3]Assistance Publique-Hôpitaux de Paris, Hôpital Necker-Enfants Malades, Service de Biochimie Métabolique, Paris, France. [4]Programme Cartes d'Identité des Tumeurs, Ligue Nationale Contre Le Cancer, Paris, France. [5]INSERM, UMR-1162, Génomique Fonctionnelle des Tumeurs Solides, Equipe Labellisée Ligue Contre le Cancer, Institut Universitaire d'Hématologie, Paris, France. [6]Université Paris 13, Sorbonne Paris Cité, Unité de Formation et de Recherche Santé, Médecine, Biologie Humaine, Bobigny, France. [7]Université Paris Diderot, Paris, France. [8]Service d'Endocrinologie, Diabète et Maladies Métaboliques, INSERM U982, Centre Hospitalier Universitaire de Rouen, Rouen Cedex, France. [9]Service d'Endocrinologie-Diabétologie-Nutrition, CHU de Rennes, Hôpital Sud, Rennes, France. [10]Service d'Endocrinologie, Hôpital Haut-Lévêque, CHU de Bordeaux, Pessac, France. [11]Service d'Endocrinologie, CHU Montpellier, Hôpital Lapeyronie, Montpellier Cedex 5, France. [12]Service d'Endocrinologie "Centre de référence maladies rares de la surrénale", Hôpital Cochin, Assistance Publique, Hôpitaux de Paris, Paris, France. [13]Centre Expert National COMETE-Cancer de la surrénale, Paris, France. [14]Assistance Publique-Hôpitaux de Paris, Hôpital Européen Georges Pompidou, Service d'hypertension artérielle et médecine vasculaire, Paris, France. [15]Assistance Publique-Hôpitaux de Paris, Hôpital Européen Georges Pompidou, Service de Génétique, Paris, France.

Note: Supplementary data for this article are available at Cancer Research Online (http://cancerres.aacrjournals.org/).

A.-P. Gimenez-Roqueplo and J. Favier jointly supervised the work.

Corresponding Authors: Judith Favier, INSERM, 56 rue Leblanc, 75015 Paris, France. Phone: 33-1-5398-8041; Fax: 33-1-5398-7952; E-mail: judith.favier@inserm.fr; and Anne-Paule Gimenez-Roqueplo, anne-paule.gimenez-roqueplo@inserm.fr

doi: 10.1158/0008-5472.CAN-17-2463

lysine demethylation of histones; ref. 4). Inhibition of PHD, TET and JmjC-domain-containing proteins respectively result in a pseudohypoxic signature and a hypermethylator phenotype (5, 6). We previously reported the first integrated multi-omics study performed on a large collection of 202 PPGL that remarkably classified tumors according to their genotype (7). Unsupervised classifications revealed that *SDHx*-mutated PPGL systematically clustered together across the genomic platforms. These tumors formed the so-called cluster 1A (pseudohypoxic) in the transcriptome study, the cluster M1 (hypermethylated) following methylome analysis and the cluster Mi1 in the miRnome-based classification (7). Intriguingly, two tumors were classified within the *SDHx*-related clusters in these data sets (Fig. 1A and B; Supplementary Fig. S1), even though both did not carry any germline or somatic *SDHx* mutations. In the first tumor, whole-exome sequencing identified the first PPGL-causative germline mutation in the *FH* gene, encoding fumarate hydratase, another TCA cycle enzyme (6) previously known to predispose to hereditary leiomyomatosis and renal cell carcinoma (HLRCC). Subsequent study identified *FH* mutations in four additional patients with PPGL, who had a high incidence of the metastatic forms of the disease (8). The aim of the present study was to identify the mutation causing the second tumor with an *SDHx*-like genomic profile.

Patients and Methods

Patients

The tumor and blood samples were prospectively collected by the French COMETE Network. This study was conducted in accordance with the Declaration of Helsinki and was approved by the local ethics committee (Comité de Protection des Personnes (CPP) Ile de France II, June 2012). Each patient signed a written informed consent for genetic analyses. The procedures used for PPGL diagnosis were in accordance with both internal and international clinical practice guidelines (2, 9). Germline DNA was extracted from leukocytes according to standard protocols. Tumor DNA extraction was performed using the AllPrep Kit (Qiagen) and the DNA Mini Kit (Qiagen) for frozen tumor and paraffin-embedded tissue, respectively. DNA was quantified and its purity assessed with a NanoDrop ND-1000 spectrophotometer (Labtech). Mutation analyses of the major PPGL susceptibility genes were performed as previously described in the Genetic department of Hôpital Européen Georges Pompidou in Paris (2). Two groups of patients for whom no known mutation in a PPGL predisposition gene had been identified were enrolled: a first group of 267 patients with a clinical history suggestive of a hereditary PPGL (multiple tumors, early onset or family history of PPGL) and a second group of 372 patients with apparently sporadic PPGL (Table 1).

Whole-exome sequencing

Exome sequencing was performed by IntegraGen Genomics (Evry, France) as previously described (6). The germline mutation identified in the *SLC25A11* gene was validated by Sanger sequencing.

Next-generation sequencing on known PPGL susceptibility genes

PPGL susceptibility genes coding regions and exon-intron boundaries (*SDHx*, *VHL*, *EPAS1*, *EGLN1*, *EGLN2*, *NF1*, *RET*, *TMEM127*, *MAX*, *FH* and *MDH2* genes) were amplified using the SDH MASTR Kit V2.0 (Multiplicom, Belgium). Libraries were sequenced on MiSeq platform (Illumina) using v3 chemistry according to the standard protocol. Alignment and variant calling were performed using SeqNEXT (JSI medical systems) and PolyDiag (Paris Descartes university) software.

Genome editing in *SLC25A11* gene by the CRISPR–Cas9 method

Targeted gRNA was designed *in silico* by using http://crispr.genome-engineering.org/ as previously described (10). gRNA was transcribed *in vitro* using the kit PrecisionX Cas9 SmartNuclease RNA system (System Biosciences CAS510A-KIT). Briefly, targeted oligonucleotides were annealed to form double strands, and then cloned into SmartNuclease Linearized T7 gRNA Vector. The resulting recombinant vector was linearized by EcoRI digestion. The generated template was used to produce gRNA by *in vitro* transcription. gRNA was then purified (miRNeasy minikit, Qiagen) and its purity was assessed using the Experion RNA StdSens Analysis Kit (Bio-Rad).

Wild-type immortalized mouse chromaffin cells (WT imCC), previously generated by our laboratory (6), were transfected with 0.6 μg of gRNA (RNA i-MAX; Life Technologies) and 2 μg of Cas9 (System Biosciences CAS940A-1) and YFP plasmids (Lipofectamine 2000; Life Technologies). Fluorescent cells were cloned by FACS sorting. Clones were screened by direct sequencing of the targeted sequence of murine *Slc25a11* gene. Two consecutive transfections were performed: the first generated three heterozygous clones out of 70, and the second performed on heterozygous clones generated 51 homozygous clones out of 129. Predicted exonic off-target sequences were screened by direct sequencing (*KRT9* exon 2, *TMEM260* exon 16, *ALDH2* exon 10, *KANK1* exon 19, *FCRLB* exon 2). *Mycoplasma* contamination was ruled out using the PCR *Mycoplasma* Test kit I/C (PromKine, PK-CA91-1048). All experiments were performed between passages 15 and 20.

Slc25a11$^{\Delta/\Delta}$ clones transfection by *Slc25a11* plasmid

Slc25a11$^{\Delta/\Delta}$ clone 6 was transfected with 2 μg of *Slc25a11*-expressing vector (ORIGENE, MR204477) using Lipofectamine 2000 (Life Technologies). Twenty-four hours later, selection was performed by Geneticin (Sigma, G8168, 800 μg/mL) and selected cells were cloned by limited dilution under Geneticin selection.

5-methylcytosine and 5-hydroxymethylcytosine ELISA

200 ng of denatured DNA was added to the Reacti-Bind Coating Solution (Thermo, 17250) and incubated in a 96-well plate at 37°C for one hour. After blocking for 30 minutes with a blocking buffer [PBS1X, 5 g/l BSA, and 0,5% of Kathon CG/ICP (Supelco 5-0127)], anti-5-methylcytosine (1/5,000, Calbiochem, NA81) or anti 5-hydroxy-methylcytosine (1/200, Actif Motif, 39759) and secondary antibody (1/1,000) were added to the wells and incubated at 37°C overnight. The plate was then incubated with Streptavidin-HRP (BD Biosciences, 554066) for 30 minutes. Finally, revelation was performed by adding a solution of 5 mg/mL of TMB (Sigma), citrate 0,1 mol/L pH 5 and 3% hydrogen peroxide. Reaction was stopped with sulfuric acid and the absorbance was read at 450 nm. The experiments were performed three times.

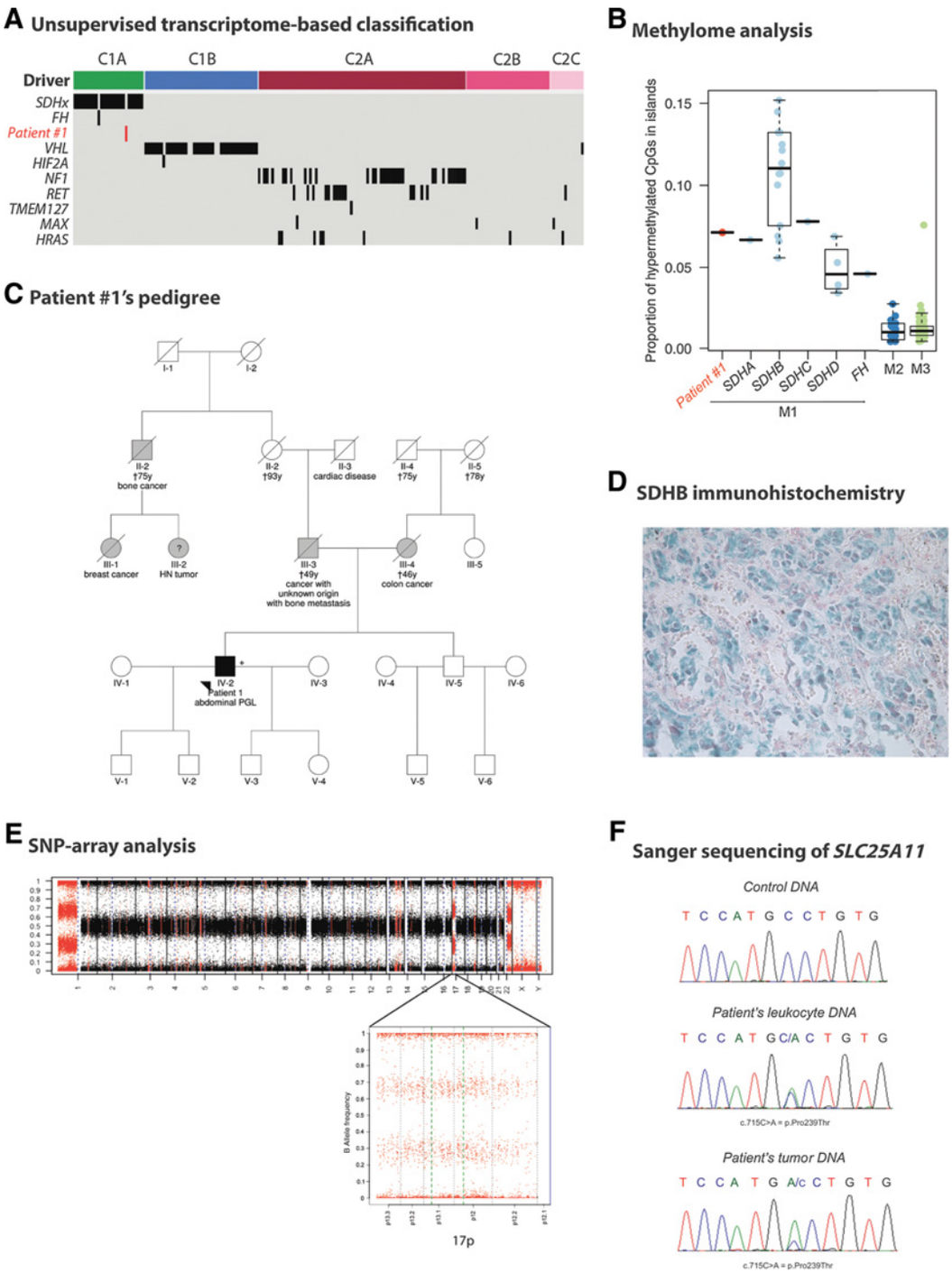

Figure 1.

Identification of an *SLC25A11* mutation in a patient with a paraganglioma. **A,** Transcriptome-based classification of 188 PPGL collected by the COMETE cohort reveals five clusters strongly associated with driver mutations. The paraganglioma of patient #1 classifies within cluster C1A together with *SDHx*- and *FH*-mutated tumors. **B,** The proportion of probes located within CpG islands that are hypermethylated with respect to normal samples (beta value difference > 0.2) is represented as a function of tumor subtype. Hypermethylated (M1) tumors are divided according to the mutated driver gene. The paraganglioma of patient #1 classifies within cluster M1 together with *SDHx*- and *FH*-mutated tumors. **C,** Pedigree of patient #1 (black box) shows several cases of cancers (gray boxes) in his family. **D,** Positive SDHB IHC of the patient #1's paraganglioma. **E,** B alleles frequency plots generated by SNP array analysis of the patient #1's paraganglioma show a 17p copy neutral LOH. **F,** Electropherograms of Sanger sequencing of the exon 6 of *SLC25A11* gene showing the c.715C>A mutation at heterozygous state from germline and at homozygous state from tumor DNA of patient #1 compared with a control DNA.

Table 1. Main clinical and tumor features of patients from the validation cohort

Clinical feature	Number of patients	Percentage
Benign PPGL	**518**	**81%**
Single HN PGL	74	
Single TAP PGL	180	
Single PCC	189	
Unknown localization	1	
Multiple HN PGL	25	
Multiple TAP PGL	12	
Bilateral PCC	17	
HN + TAP PGL	5	
PCC + TAP PGL	14	
Unknown localization	1	
Metastatic PPGL	**121**	**19%**
Single HN PGL	13	
Single TAP PGL	32	
Single PCC	66	
Unknown localization	3	
Multiple HN PGL	1	
Multiple TAP PGL	2	
Bilateral PCC	3	
PCC + TAP PGL	1	
	639	

Abbreviations: HN, head and neck PGL; PCC, pheochromocytoma; TAP, thoracic and abdominopelvic PGL.

Statistical analysis

Data were analyzed by one-way ANOVA. The results were considered to be significant if $P < 0.05$. Statistics tests were carried out using the Graph-Pad software.

Results

Characterization of the unexplained *SDHx*-like tumor

The unexplained tumor with a pseudo-*SDHx* profile (Fig. 1A and B; Supplementary Fig. S1) was a nonsecreting abdominal paraganglioma diagnosed in a 46 years-old patient (Patient #1). Genetic counseling revealed a family history of cancer, with his father deceased at 49 from a cancer of unknown origin discovered by bone metastases, a paternal uncle with bone cancer, and a paternal cousin with a head and neck tumor (Fig. 1C). Unfortunately, it was not possible to retrieve neither more specific clinical information regarding the relatives of the paternal branch suspected to be affected, nor tumors or DNA samples. Patient #1's tumor was positive for SDHB by immunochemistry (Fig. 1D) confirming the absence of *SDHx* mutations (11). Whole-exome sequencing performed on leukocyte DNA identified 2,343 germline genetic variations (2,213 SNVs and 130 InDels). After filtration of the common polymorphisms described in the dbSNP, ExAC or 1000 Genome databases, 218 variations remained. We hypothesized that similar to *SDHx* and *FH* genes, the causative gene could be a tumor suppressor, and searched for variations associated with a loss of heterozygosity (LOH) using SNP array in tumor DNA (Fig. 1E). We found 54 variations, of which 11 were classified as pathogenic according to *in silico* analyses (Supplementary Table S1). Among them, we identified a candidate genetic variation [c.715C>A, p.(Pro239Thr)] in the *SLC25A11* gene (NM_003562), encoding the mitochondrial 2-oxoglutarate/malate carrier (OGC) protein. The presence of the *SLC25A11* variation, heterozygous in germline and homozygous in tumor DNA, was confirmed by Sanger sequencing (Fig. 1F). OGC is part of the malate/aspartate shuttle (MAS) and mediates the transport of 2-OG from the mitochondrial matrix to the cytoplasm in an electroneutral exchange for malate (Fig. 2A). The proline at position 239 is part of a PX[D/E]XX[K/R]X[K/R] signature sequence motif (PROSITE PS50920, PFAM PF00153), which is highly conserved across species, particularly in the SLC25 family of mitochondrial transporters (12). Mutagenesis of this amino acid in bovine OGC results in a severe defect of 2-OG transport activity (12). We performed OGC immunohistochemistry (IHC)

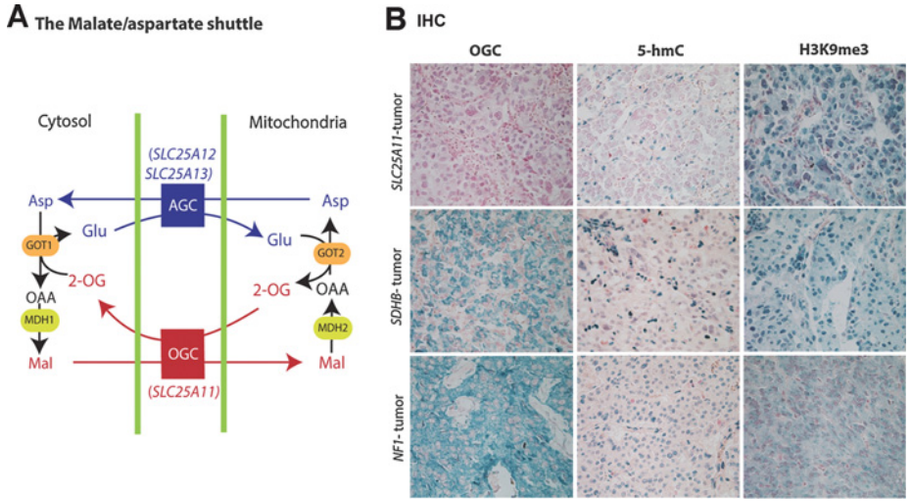

Figure 2.

SLC25A11 mutation is associated with loss of OGC, hypermethylator phenotype, and metabolic reprogramming. **A,** Schematic presentation of the malate–aspartate shuttle, composed of the OGC (encoded by *SLC25A11*) and the aspartate–glutamate carriers (AGC, encoded by *SLC25A12* and *13* genes). Asp, aspartate; Glu, glutamate; Mal, malate; OAA, oxaloacetate. **B,** OGC IHC in the *SLC25A11*-mutated paraganglioma from patient #1 shows no immunostaining, whereas a strong granular staining expected from a mitochondrial protein is observed in *SDHB* and *NF1*-mutated tumors. 5-hmC and H3K9 IHC in *SLC25A11*-mutated paraganglioma from patient #1 show an immunostaining, suggesting DNA and histone methylation.

Table 2. Clinical, genetic, and immunohistological characteristics of *SLC25A11* mutation carriers

	Sex	Age	Tumor location	Meta	Delay for meta diagnosis	Secretion	cDNA mutation	Protein alteration	LOH	OGC IHC	5-hmC IHC	H3me3 IHC
Patient #1	M	46	A PGL	No	NA	No	c.715C>A	p.(Pro239Thr)	Yes	Neg	Neg	Pos
Patient #2	F	51	A PGL	Yes	sync	NM	c.439A>G	p.(Met147Val)	Yes	Neg	Pos	Pos
Patient #3	M	67	A PGL	Yes	3 years	NM	c.248+3A>G	p.?	ND	ND	ND	ND
Patient #4	F	32	HN PGL	No	NA	No	c.708C>T	p.(Ala236Ala)	Yes	Neg	Neg	Pos
Patient #5	F	87	A PGL	Yes	sync	NM	c.25delG	p.(Ala9ProfsTer4)	ND	ND	ND	ND
Patient #6	F	59	A PGL	Yes	3 years	NM	c.421G>A	p.(Glu141Lys)	Yes	Neg	Neg	Pos
Patient #7	F	74	A PGL	Yes	sync	NM	c.107_108del	p.(Thr36SerfsTer71)	Yes	Neg	Neg	Pos

Abbreviations: Meta, metastases; A PGL, abdominal paraganglioma; HN PGL, head and neck paraganglioma; sync, synchronous; NM, normetanephrines; LOH, Loss of heterozygosity; H3me3, H3K9me3 and H3K27me3; Neg, negative; Pos, positive; ND, not determined; NA, not applicable.

on the paraffin-embedded tumor. We observed no OGC protein in the PGL carrying the *SLC25A11* mutation in contrast with the 20 PPGL tumors without *SLC25A11* mutations used as controls (6 *SDHx*, 1 *FH*, 3 *RET*, 4 *NF1*, 1 *TMEM127*, 3 *MAX*, 2 sporadic cases; Fig. 2B; Supplementary Table S2). 5-hmC and H3K9me3 IHC further validated a hypermethylated phenotype affecting both DNA and histones, as previously described in *SDHx*-mutated tumors (6, 13). Altogether these data suggested that germline [c.715C>A, p.(Pro239Thr)] *SLC25A11* mutation associated with somatic loss of the wild-type allele causes the patient's PGL.

SLC25A11 gene sequencing on a large cohort of PPGL

To establish the frequency of *SLC25A11* mutations in patients with PPGL, the 8 exons and exon/intron junctions of the gene were sequenced by Sanger method in a large cohort of 639 patients for whom no germline mutation had been identified in the major PPGL susceptibility genes (*SDHx*, *RET*, *VHL*, *TMEM127*, *MAX*, *FH*), nor in the recently described *MDH2* gene (14). These patients had a mean age at diagnosis of 34.8 years ± 15.6 (Table 1) and among them, 121 (19%) had a metastatic disease. Eighty-one (13%) had multiple PPGL and 13 (2%) reported a family history of the disease. We identified six patients with germline *SLC25A11* mutations (Table 2; Supplementary Table S3). Five patients had a single metastatic abdominal PGL and one a head and neck PGL; none had a known family history of PPGL (Supplementary Fig. S2 and Supplementary Clinical Data). All six mutations (2 missense, 2 frameshifts, one intronic and one silent mutation) were predicted to be deleterious *in silico* (Table 2). None of these variants was present in the dbSNP nor ExAC databases. The missense mutations affected highly conserved amino acids (Supplementary Fig. S3A) located in the signature protein sequence or in the alpha matrix helix, both well known to be critical for OGC function (Supplementary Fig. S3B; refs. 12, 15, 16). Interestingly, the silent p.Ala236Ala mutation was associated with a marked decrease in *SLC25A11* mRNA levels in leukocytes (Supplementary Fig. S3C). LOH was identified in tumor DNA of the three patients for whom tumor tissue was available (Supplementary Fig. S3D) and all evaluable tumors were negative for OGC by IHC (Table 2; Supplementary Fig. S4). Next-generation sequencing (NGS) performed on tumor DNA of patient #1, #4 and #6 showed no somatic mutation in *SDHx*, *VHL*, *EPAS1*, *EGLN1*, *EGLN2*, *NF1*, *RET*, *TMEM127*, *MAX*, *FH* and *MDH2* genes. We had not enough material to performed NGS on PGL of patient #2. We carried out 5-hmC (Supplementary Fig. S5), H3K9me3 (Supplementary Fig. S6) and H3K27me3 IHC (Supplementary Fig. S7) to establish whether these tumors displayed a hypermethylator phenotype, as the one we observed in the initial *SLC25A11*-mutated case. In all but one of the *SLC25A11*-mutated tumors (patient #2), 5-hmC immunolabelling was less intense in tumor cells than in endothelial or sustentacular cells (Table 2; Supplementary Fig. S5), whereas H3K9me3 and H3K27me3 were positive in all cases (Table 2; Supplementary Fig. S6 and S7). Hence, *SLC25A11* mutations apparently mediate the inhibition of TET and JmjC-domain containing demethylases, as we previously reported in *SDHx*- and *FH*-mutated PPGL (6).

Slc25a11 knockout in immortalized mouse chromaffin cells

To fully demonstrate that *SLC25A11* is a new tumor-suppressor gene, we generated a knockout (KO) of the *Slc25a11* gene using the CRISPR/Cas9 approach in wild-type immortalized mouse chromaffin cells (WT imCC; ref. 6; Supplementary Fig. S8A). Two $Slc25a11^{\Delta/\Delta}$ clones (c4 and c6) were selected for analyses. These clones carried a homozygous c.720delG and a heterozygous c.720_733del14 variant in the *Slc25a11* gene (Supplementary Fig. S8B and S8C), both leading to premature stop codons in exon 7. The corresponding mutation results in the loss of the third signature sequence motif and the H56 alpha matrix helix (Supplementary Fig. S8D). A rescue was then performed by stably transfecting an *Scl25a11*-expressing vector in the $Slc25a11^{\Delta/\Delta}$clone 6 (clone c6-R). Western blot analysis of OGC protein levels revealed a loss of the transporter in both $Slc25a11^{\Delta/\Delta}$ clones, and its re-expression in the c6-R cells (Supplementary Fig. S8E). Both $Slc25a11^{\Delta/\Delta}$ clones exhibited nuclear translocation of HIF2α similar to $Sdhb^{-/-}$ cells, which was not seen in WT imCC, nor in the c6-R cells (Fig. 3A). We used an ELISA method to quantify the levels of 5-mC and 5-hmC in the different cell types. As expected, 5-mC levels were 2-fold higher in $Sdhb^{-/-}$ imCCs than in WT cells. Similarly, both $Slc25a11^{\Delta/\Delta}$ clones displayed an approximately 2-fold increase in 5-mC content, reflecting a hypermethylated phenotype, which was reversed in the *Slc25a11*-rescued cells (Fig. 3B). Accordingly, 5-hmC levels in WT imCC and c6-R were higher than in $Sdhb^{-/-}$ and $Slc25a11^{\Delta/\Delta}$ cells (Fig. 3C). Hence, *Slc25a11* inactivation promotes both a pseudohypoxic and a hypermethylated phenotype. We next evaluated the proliferation, migration and adhesion capacities of $Slc25a11^{\Delta/\Delta}$ imCCs in comparison to those of wild-type, $Sdhb^{-/-}$ and *Slc25a11*-rescued cells. *Slc25a11*-deficient cells displayed a decrease in proliferation, compared to WT cells, which was much less marked than that observed in *Sdhb*-deficient cells (Supplementary Fig. S8F). They showed increased adhesion as compared to WT cells, which was however inferior to that observed in $Sdhb^{-/-}$ imCC (Fig. 3D). *Slc25a11* KO cells demonstrated a 2-fold increase in collective migration as compared with the WT and c6-R cells and comparable with the $Sdhb^{-/-}$ imCC (Fig. 3E). Altogether, these *in vitro* data obtained with two different *Slc25a11* KO clones and the reversion of the phenotypes shown by the rescue experiments clearly demonstrate that loss of *Slc25a11* gene mediates

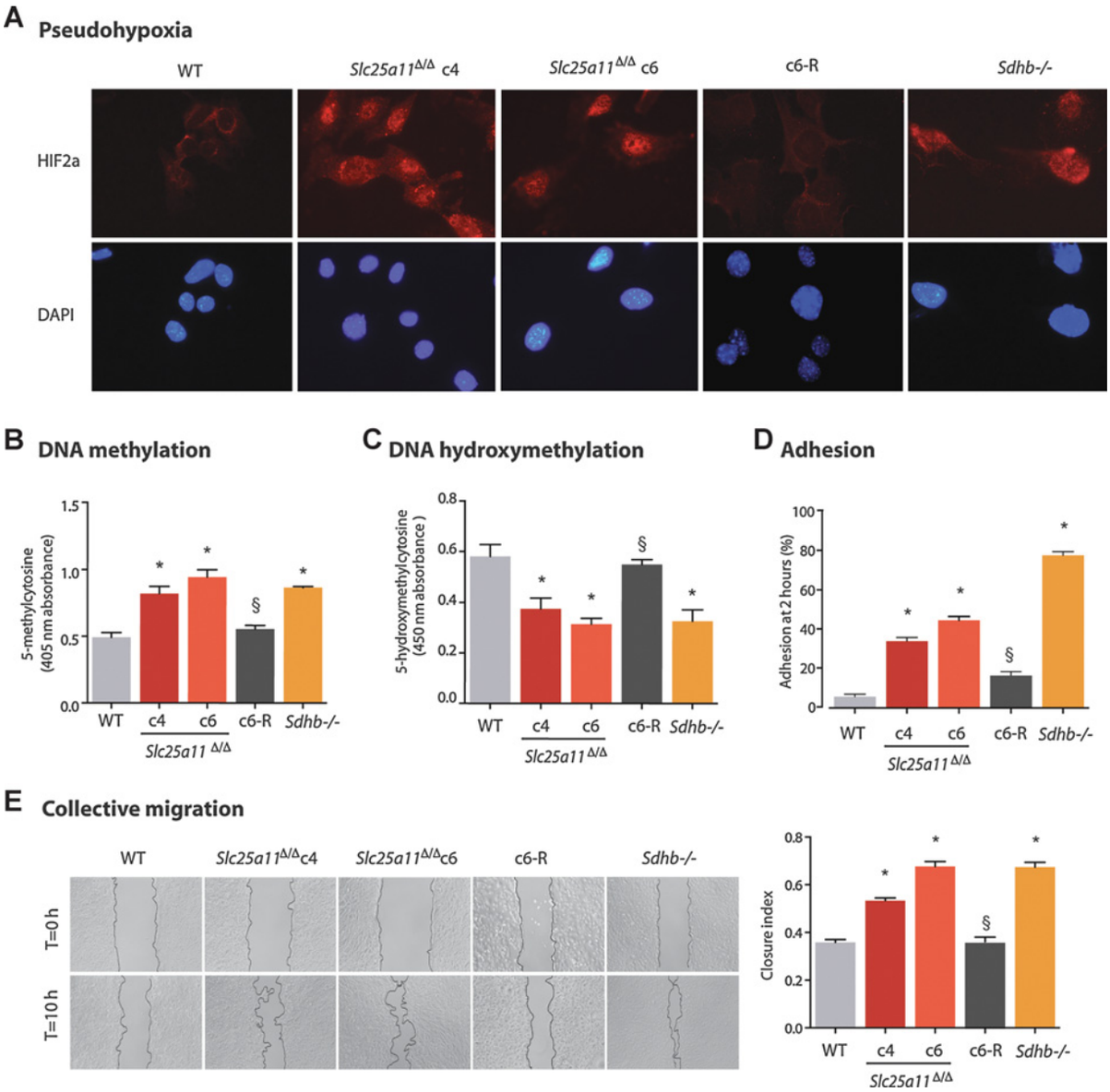

Figure 3.

Characterization of *Slc25a11*$^{\Delta/\Delta}$ immortalized mouse chromaffin cells. **A,** Immunofluorescence showing HIF2 nuclear localization in *Slc25a11*$^{\Delta/\Delta}$ (clones c4 and c6) and *Sdhb*$^{-/-}$ imCCs, whereas the signal is restricted to the cytoplasm in WT cells and *SLC25A11* rescued cells (c6-R). **B,** 5-methylcytosine quantification by ELISA in all cell types reveals the hypermethylator phenotype of *Slc25a11*$^{\Delta/\Delta}$ *cells* at comparable level with that observed in *Sdhb*-deficient imCCs. **C,** 5-hydroxymethylcytosine quantification by ELISA in all cell types shows a decrease level of 5-hmC quantification in *Slc25a11*-deficient cells at comparable level with *Sdhb*-deficient imCCs. **D,** Increased adhesion in *Slc25a11*$^{\Delta/\Delta}$ and *Sdhb*$^{-/-}$ as compared with WT and c6-R imCCs. **E,** Scratch test experiments reveal that collective migration is increased in *Slc25a11*$^{\Delta/\Delta}$ and *Sdhb*$^{-/-}$ imCCs compared with WT and c6-R cells. Data are mean ± SEM; *, $P < 0.01$ versus WT; §, $P < 0.01$ c4 and c6 versus c6R.

pseudo-hypoxic signature, hypermethylator phenotype and the acquisition of metastatic properties.

To decipher the mechanism linking SLC25A11 loss of function and this phenotype, we performed metabolomic analysis in the different cell types, which showed normal levels of succinate (Supplementary Fig. S8G) but higher levels of aspartate and glutamate, and lower levels of 2-OG in *Slc25a11*$^{\Delta/\Delta}$ cells (Fig. 4A). Interestingly, treating *Slc25a11*$^{\Delta/\Delta}$ cells with 2-OG reversed the migratory phenotype, demonstrating the role of this metabolite in the SLC25A11 tumorigenic cascade (Fig. 4B). Metabolomic analysis performed on the frozen tumor of patients #1, #6 and #7 showed normal succinate levels (Supplementary Fig. S9) whereas, consistent with MAS dysfunction and *in vitro* data, aspartate and glutamate concentrations were elevated in all three *SLC25A11*-mutated tumors compared with control PPGL samples from the cluster 1A (2 *SDHB* and 1 *SDHD*-mutated cases)

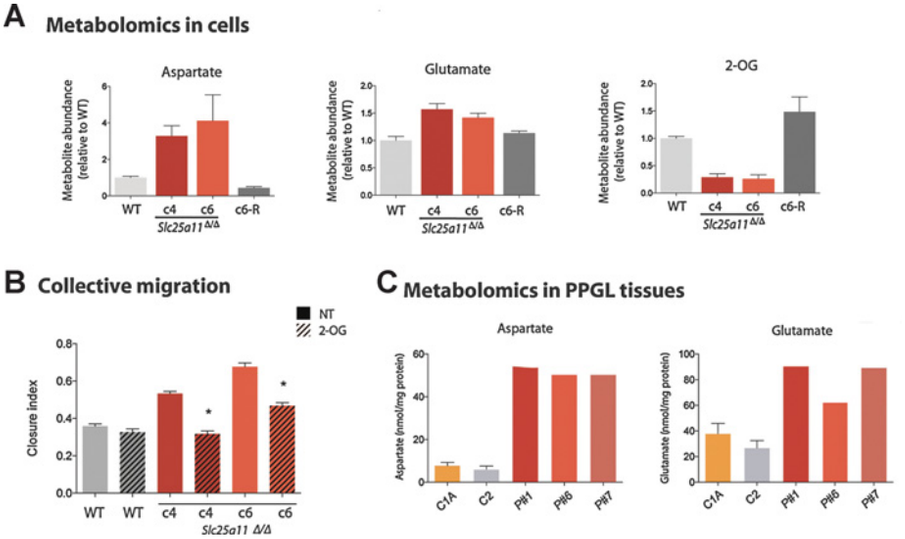

Figure 4.

A, Metabolomic profiling in the different cell types shows increased levels of intracellular aspartate and glutamate in *Slc25a11*-deficient cells (clones c4 and c6) versus WT, whereas 2-OG is decreased in *Slc25a11*$^{\Delta/\Delta}$ cells. Aspartate and glutamate both decrease, whereas 2-OG increases in *SLC25A11* rescued cells (c6-R). **B,** 2-OG treatment (hashed bars) reverses the collective migration capacities of *Slc25a11*-deficient cells (clones c4 and c6). **C**, Metabolomic analysis of the *SLC25A11*-mutated paraganglioma of patients #1, #6, and #7 reveals that aspartate and glutamate steady-state levels are increased as compared with control tumors from the cluster 1A (2 *SDHB*, 1 *SDHD* PPGL) or the cluster 2 (3 *RET*, 1 *TMEM127*, 1 sporadic PPGL). *, $P < 0.01$ versus WT.

or the cluster 2 (3 *RET*, 1 *TMEM127* and 1 sporadic case; Fig. 4C). 2-OG levels were highly variable between tumors homogenates and did not show such decrease (Supplementary Fig. S9).

Discussion

We identified *SLC25A11* as a new tumor-suppressor gene implicated in the predisposition to metastatic paraganglioma. This gene encodes a carrier that participates to malate–asparate shuttle (MAS) by mediating the transport of 2-OG from the mitochondrial matrix to the cytoplasm in an electroneutral exchange with malate. MAS is composed of OGC (*SLC25A11*) and of two aspartate–glutamate carriers: CITRIN *(SLC25A13)* and ARALAR (*SLC25A12*; Fig. 2). This shuttle regenerates NADH pool in mitochondrial matrix to allow complex I function (17). After the identification of 7 PPGL predisposing genes encoding TCA cycle enzymes *(SDHA, B, C, D, SDHAF2, FH* and *MDH2)*, it is the first time that a gene encoding a mitochondrial carrier is implicated in PPGL tumorigenesis. Interestingly, patients with CITRIN deficiency caused by homozygous germline mutation in *SLC25A13* have an increased risk of hepatocellular carcinoma following hepatic inflammation and fibrosis (18). Also, heterozygous germline mutations in the *SLC25A13* gene have been implicated in hepatocellular carcinoma in Asiatic population, suggesting a potential role for MAS in tumorigenesis (19). Nevertheless, mutations in *SLC25A13* reported in the latter study are frequent in Asiatic population raising the question of their actual pathogenicity (20).

More strikingly, a gain-of-function mutation in the *GOT2* gene, encoding the mitochondrial aspartate aminotransferase was very recently reported in a PGL patient, further reinforcing the link between MAS dysfunction and PPGL (21). The aspartate aminotransferase catalyzes the interconversion of aspartate and 2-OG to oxaloacetate and glutamate. Our metabolomics data show a marked increase in aspartate and glutamate in both *SLC25A11*-mutated human samples and KO mouse cells associated with a decrease in 2-OG in the KO cells. Various derivatives of glutamate and aspartate were previously shown to be potent inhibitors of HIF prolyl hydroxylases (22). Furthermore, these changes associated with the decrease in 2-OG levels may suggest an increased GOT2 activity in *SLC25A11*-deficent cells. This could lead to an alteration of the 2-OG/succinate ratio and to the subsequent inhibition of 2-OG dependent enzymes. This is consistent with the recent data on *GOT2* activating mutation, where the aspartate/glutamate ratio is also increased (21). Hence, although further studies will be needed, these observations may explain the link between MAS dysfunction and tumorigenesis.

We show that *SLC25A11* gene mutations account for 1% of all PPGL, a frequency equivalent to the recently identified PPGL susceptibility genes (*SDHA*, *TMEM127*, *MAX*, *FH*; refs. 1, 8, 14). Although these data will need to be confirmed in an independent cohort, our analysis of more than 600 patients does suggest that *SLC25A11* gene should now be screened in patients with PPGL, especially for those with a malignant phenotype. It is still unclear what will be the penetrance of the disease in affected families. The information we could obtain on few relatives of the *SLC25A11*-mutation carriers were suggestive of family history of cancers (cases reported with bone metastases of unknown primitive cancer, leukemia, as well as colon, breast, prostate and throat cancers) but not precise enough to allow drawing definite conclusions. So, it should further be assessed whether *SLC25A11*-mutations may confer an increased risk to other type of cancers. Moreover, *SLC25A11* somatic mutations or copy-number alterations have been reported in various types of cancers in The Cancer Genome Atlas (TCGA) project or the Catalog Of Somatic Mutations In Cancer (COSMIC) database (Supplementary Table S4), and 33 of these 145 samples were shown to present an underexpression of *SLC25A11* mRNA, thus strengthening the hypothesis of a role of *SLC25A11* in the tumorigenesis of other types of cancers. Interestingly, a low expression of *SLC25A11* is associated with a reduced survival in renal and pancreatic cancers, according to the TCGA studies (23).

It is worth noting that *SLC25A11* gene mutations are strongly associated with the development of metastatic PPGL as 5% of all metastatic patients in our cohort were *SLC25A11* mutations carriers and a malignant phenotype was observed in 5 out of the

7 (71%) *SLC25A11* mutation carriers (Table 2). In particular, we found germline *SLC25A11* mutations in 5 out of 30 (17%) patients with a single, apparently sporadic metastatic abdominal PGL (Table 1). In PPGL, malignancy diagnosis is made at the time of the diagnosis of the first metastasis (24) and the identification of an *SDHB* or an *FH* mutation are a risk factor for malignant disease. This study suggests that similar to *SDHB* and *FH* mutations, *SLC25A11* could be considered as a new genetic risk factor of metastatic PPGL. This observation is important for the follow-up of mutation carriers and may also have some important consequences on their therapeutic management. *SDHx*, *FH*- and now *SLC25A11*-mutated tumors should be managed as the so-called 'Cluster 1A' associated tumors. They display pseudo-hypoxic and hypermethylator phenotypes that probably participate to the acquisition of some metastatic properties (6, 25). Hence, antiangiogenic therapies or demethylating agents such as low-dosed 5-aza-deoxycytidine may be of therapeutic benefit for these specific patients. Similarly, it has recently been shown that *MGMT* promoter methylation in *SDHB*-metastatic PPGL confers an increased response to temozolomide (6, 26). Hence, *SCL25A11*-mutated carriers may also benefit from such therapy.

In conclusion, we show, using a large cohort of affected patients and an *in vitro* experimental model generated by CRISPR/Cas9 technology, that *SLC25A11* is a new tumor-suppressor gene conferring a predisposition to metastatic PPGL. The data reported here show how a mitochondrial dysfunction driven by a transporter inactivation can lead to tumorigenesis, and further broadens the field of mitochondrial genetic defects and cancer.

Disclosure of Potential Conflicts of Interest

No potential conflicts of interest were disclosed.

Authors' Contributions

Conception and design: A. Buffet, N. Burnichon, A.-P. Gimenez-Roqueplo, J. Favier

Development of methodology: A. Morin, J. Favier

Acquisition of data (provided animals, acquired and managed patients, provided facilities, etc.): L.-J. Castro-Vega, F. Habarou, C. Lussey-Lepoutre, E. Letouzé, H. Lefebvre, I. Guilhem, M. Haissaguerre, M. Padilla-Girola, T. Tran, L. Tchara, J. Bertherat, L. Amar, C. Ottolenghi, A.-P. Gimenez-Roqueplo

Analysis and interpretation of data (e.g., statistical analysis, biostatistics, computational analysis): A. Buffet, L.-J. Castro-Vega, F. Habarou, E. Letouzé, N. Burnichon, A.-P. Gimenez-Roqueplo, J. Favier

Writing, review, and/or revision of the manuscript: A. Buffet, L.-J. Castro-Vega, F. Habarou, I. Raingeard, J. Bertherat, N. Burnichon, A.-P. Gimenez-Roqueplo, J. Favier

Administrative, technical, or material support (i.e., reporting or organizing data, constructing databases): A.-P. Gimenez-Roqueplo

Study supervision: A.-P. Gimenez-Roqueplo, J. Favier

Acknowledgments

We thank Profs. Pierre-François Plouin and Xavier Bertagna for making this work possible through the COMETE Network. We also thank Jean-Michael Mazzella, Mélanie Menara, Aurélien de Reyniès, Nabila Elarouci, Dr. Rossella Libé, Prof. Antoine Tabarin, Prof. Cécile Badoual, Dr Tchao Méatchi, Dr. Mathilde Sibony, Dr Frédérique Tissier, Prof. Nathalie Rioux-Leclercq, Dr. François Le Gall, Dr. Françoise Gobet, Prof. Béatrice Vergier, Dr. Isabelle Pellegrin, Dr. Joel Edery, and Dr. Nathalie Carrere for their help, Estelle Robidel, Maëva Ruel, Irmine Ferrara, Stefani Mazurkiewics, Christophe Simian and Marie Fontenille for technical assistance, Catherine Tritscher for administrative assistance and Pr. Bertrand Tavitian for helpful discussion. We also thank all members of the Genetics Department and Biological Resources Center and Tumor Bank Platform, Hôpital européen Georges Pompidou (BB-0033-00063), all the members of the Tumor BioBank-biological resource center of Rouen University Hospital, all the members of the Centre de Ressources Biologiques Plurithématique Bordeaux Biothèques Santé (BB-0033-00036) and the Mass spectrometry platform of the Biology Department of the Necker Hospital (Christophe Merlette). This work has received funding from the Agence Nationale de la Recherche (ANR-2011-JCJC-00701 MODEOMAPP), the European Union Seventh Framework Program (FP7/2007-2013) under grant agreement n° 259735, the Plan Cancer: Appel à projets Epigénétique et Cancer 2013 (EPIG201303 METABEPIC), the European Union's Horizon 2020 research and innovation program under grant agreement No 633983 and by the Institut National du Cancer and the Direction Générale de l'Offre de Soins (PRT-K 2014, COMETE-TACTIC, INCa-DGOS_8663). A. Buffet received a financial support from ITMO Cancer AVIESAN (Alliance Nationale pour les Sciences de la Vie et de la Santé, National Alliance for Life Sciences & Health) within the framework of the Cancer Plan and from la Fondation pour la Recherche Médicale (FDT20170436955). C. Lussey-Lepoutre and N. Burnichon are funded by the Cancer Research for Personalized Medicine - CARPEM project (Site de Recherche Intégré sur le Cancer - SIRIC). The group is supported by the Ligue Nationale contre le Cancer (Equipe Labellisée). This work is part of the "Cartes d'Identité des Tumeurs (CIT) program" funded and developed by the `Ligue Nationale contre le Cancer' (http://cit.ligue-cancer.net).

The costs of publication of this article were defrayed in part by the payment of page charges. This article must therefore be hereby marked *advertisement* in accordance with 18 U.S.C. Section 1734 solely to indicate this fact.

Received August 15, 2017; revised December 14, 2017; accepted January 31, 2018; published first February 5, 2018.

References

1. Favier J, Amar L, Gimenez-Roqueplo AP. Paraganglioma and phaeochromocytoma: from genetics to personalized medicine. Nat Rev Endocrinol 2015;11:101–11.
2. Burnichon N, Rohmer V, Amar L, Herman P, Leboulleux S, Darrouzet V, et al. The succinate dehydrogenase genetic testing in a large prospective series of patients with paragangliomas. J Clin Endocrinol Metab 2009; 94:2817–27.
3. Pastor WA, Aravind L, Rao A. TETonic shift: biological roles of TET proteins in DNA demethylation and transcription. Nat Rev Mol Cell Biol 2013; 14:341–56.
4. Klose RJ, Kallin EM, Zhang Y. JmjC-domain-containing proteins and histone demethylation. Nat Rev Genet 2006;7:715–27.
5. Selak MA, Armour SM, MacKenzie ED, Boulahbel H, Watson DG, Mansfield KD, et al. Succinate links TCA cycle dysfunction to oncogenesis by inhibiting HIF-alpha prolyl hydroxylase. Cancer Cell 2005;7:77–85.
6. Letouze E, Martinelli C, Loriot C, Burnichon N, Abermil N, Ottolenghi C, et al. SDH mutations establish a hypermethylator phenotype in paraganglioma. Cancer Cell 2013;23:739–52.
7. Castro-Vega LJ, Letouze E, Burnichon N, Buffet A, Disderot PH, Khalifa E, et al. Multi-omics analysis defines core genomic alterations in pheochromocytomas and paragangliomas. Nat Commun 2015;6:6044.
8. Castro-Vega LJ, Buffet A, De Cubas AA, Cascon A, Menara M, Khalifa E, et al. Germline mutations in FH confer predisposition to malignant pheochromocytomas and paragangliomas. Hum Mol Genet 2014;23:2440–6.
9. Lenders JW, Duh QY, Eisenhofer G, Gimenez-Roqueplo AP, Grebe SK, Murad MH, et al. Pheochromocytoma and paraganglioma: an endocrine society clinical practice guideline. J Clin Endocrinol Metab 2014;99: 1915–42.
10. Hsu PD, Scott DA, Weinstein JA, Ran FA, Konermann S, Agarwala V, et al. DNA targeting specificity of RNA-guided Cas9 nucleases. Nat Biotechnol 2013;31:827–32.

11. Menara M, Oudijk L, Badoual C, Bertherat J, Lepoutre-Lussey C, Amar L, et al. SDHD immunohistochemistry: a new tool to validate SDHx mutations in pheochromocytoma/paraganglioma. J Clin Endocrinol Metab 2015;100:E287–91.
12. Cappello AR, Curcio R, Valeria Miniero D, Stipani I, Robinson AJ, Kunji ER, et al. Functional and structural role of amino acid residues in the even-numbered transmembrane alpha-helices of the bovine mitochondrial oxoglutarate carrier. J Mol Biol 2006;363:51–62.
13. Killian JK, Kim SY, Miettinen M, Smith C, Merino M, Tsokos M, et al. Succinate dehydrogenase mutation underlies global epigenomic divergence in gastrointestinal stromal tumor. Cancer Discov 2013;3:648–57.
14. Cascon A, Comino-Mendez I, Curras-Freixes M, de Cubas AA, Contreras L, Richter S, et al. Whole-exome sequencing identifies MDH2 as a new familial paraganglioma gene. J Natl Cancer Inst 2015;107.
15. Miniero DV, Cappello AR, Curcio R, Ludovico A, Daddabbo L, Stipani I, et al. Functional and structural role of amino acid residues in the matrix alpha-helices, termini and cytosolic loops of the bovine mitochondrial oxoglutarate carrier. Biochim Biophys Acta 2011;1807:302–10.
16. Stipani V, Cappello AR, Daddabbo L, Natuzzi D, Miniero DV, Stipani I, et al. The mitochondrial oxoglutarate carrier: cysteine-scanning mutagenesis of transmembrane domain IV and sensitivity of Cys mutants to sulfhydryl reagents. Biochemistry 2001;40:15805–10.
17. Monne M, Palmieri F. Antiporters of the mitochondrial carrier family. Curr Top Membr 2014;73:289–320.
18. Ohura T, Kobayashi K, Tazawa Y, Nishi I, Abukawa D, Sakamoto O, et al. Neonatal presentation of adult-onset type II citrullinemia. Hum Genet 2001;108:87–90.
19. Chang KW, Chen HL, Chien YH, Chen TC, Yeh CT. SLC25A13 gene mutations in Taiwanese patients with non-viral hepatocellular carcinoma. Mol Genet Metab 2011;103:293–6.
20. Dong H, Zhang H, Liang J, Yan H, Chen Y, Shen Y, et al. Digital karyotyping reveals probable target genes at 7q21.3 locus in hepatocellular carcinoma. BMC Med Genet 2011;4:60.
21. Remacha L, Comino-Mendez I, Richter S, Contreras L, Curras-Freixes M, Pita G, et al. Targeted exome sequencing of Krebs cycle genes reveals candidate cancer predisposing mutations in pheochromocytomas and paragangliomas. Clin Cancer Res 2017;23:6315–24.
22. Mole DR, Schlemminger I, McNeill LA, Hewitson KS, Pugh CW, Ratcliffe PJ, et al. 2-oxoglutarate analogue inhibitors of HIF prolyl hydroxylase. Bioorg Med Chem Lett 2003;13:2677–80.
23. Chandrashekar DS, Bashel B, Balasubramanya SAH, Creighton CJ, Ponce-Rodriguez I, Chakravarthi B, et al. UALCAN: a portal for facilitating tumor subgroup gene expression and survival analyses. Neoplasia 2017;19:649–58.
24. Gimenez-Roqueplo AP, Favier J, Rustin P, Rieubland C, Crespin M, Nau V, et al. Mutations in the SDHB gene are associated with extra-adrenal and/or malignant phaeochromocytomas. Cancer Res 2003;63:5615–21.
25. Loriot C, Domingues M, Berger A, Menara M, Ruel M, Morin A, et al. Deciphering the molecular basis of invasiveness in Sdhb-deficient cells. Oncotarget 2015;6:32955–65.
26. Hadoux J, Favier J, Scoazec JY, Leboulleux S, Al Ghuzlan A, Caramella C, et al. SDHB mutations are associated with response to temozolomide in patients with metastatic pheochromocytoma or paraganglioma. Int J Cancer 2014;135:2711–20.